Development 139, 1141-1152 (2012) doi:10.1242/dev.072439

The metalloproteinase inhibitor Reck is essential for zebrafish DRG development

Andrew Prendergast[1,3], Tor H. Linbo[3], Tanya Swarts[3], Josette M. Ungos[2,3], Hillary F. McGraw[2,3], Shlomo Krispin[4], Brant M. Weinstein[4] and David W. Raible[1,2,3,*]

SUMMARY

The neural crest is a migratory, multipotent cell lineage that contributes to myriad tissues, including sensory neurons and glia of the dorsal root ganglia (DRG). To identify genes affecting cell fate specification in neural crest, we performed a forward genetic screen for mutations causing DRG deficiencies in zebrafish. This screen yielded a mutant lacking all DRG, which we named *sensory deprived* (*sdp*). We identified a total of four alleles of *sdp*, all of which possess lesions in the gene coding for reversion-inducing cysteine-rich protein containing Kazal motifs (Reck). Reck is an inhibitor of metalloproteinases previously shown to regulate cell motility. We found *reck* function to be both necessary for DRG formation and sufficient to rescue the *sdp* phenotype. *reck* is expressed in neural crest cells and is required in a cell-autonomous fashion for appropriate sensory neuron formation. In the absence of *reck* function, sensory neuron precursors fail to migrate to the position of the DRG, suggesting that this molecule is crucial for proper migration and differentiation.

KEY WORDS: *reck*, Neural crest, Neurogenesis, Zebrafish

INTRODUCTION

During normal embryonic development, cells are often generated in locations far removed from their place of differentiation. Cell migration is important in the formation of many tissues, and the dysregulation of migration has drastic consequences for embryos and adult organisms alike. Neural crest is a transient cell lineage that gives rise to tissues including but not limited to: cartilage and bone of the craniofacial skeleton, secretory neuroendocrine cells, pigment cells, and many of the neurons and glia of the peripheral nervous system (Le Douarin and Kalcheim, 1999). Neural crest is specified as a limited cell population at the lateral border of neural and non-neural ectoderm; it must then migrate in regulated phases and expand to generate these derivatives. All vertebrate taxa possess neural crest, and the mechanisms that distinguish neural crest from all other cell types are considered to have been critical in the origin and evolution of the vertebrate clade (Gans and Northcutt, 1983; Knecht and Bronner-Fraser, 2002).

The relationship between neural crest differentiation and migration is poorly understood. Most studies have identified molecules crucial to early events in migration, such as delamination from the neuroectoderm or maintenance of neural crest segmentation. However, little attention has been paid to the cues that terminate migration, an essential condition for appropriate neural crest cell differentiation. Furthermore, although studies have defined a handful of guidance factors and extracellular matrix cues that direct neural crest to its targets, it is unclear how these migratory cues interact with specific neural crest fate decisions.

Dorsal root ganglia (DRG) are a crest-derived, segmentally arrayed series of sensory neurons and their associated glia that detect pain, temperature, mechanical and proprioceptive stimuli. Expression of the Neurogenins (Neurog), a family of basic helix-loop-helix (bHLH) transcription factors, is currently the earliest known indicator of DRG neuronal identity (Greenwood et al., 1999; Ma et al., 1999; Perez et al., 1999). In the zebrafish, *neurog1* is essential for the formation of DRG neurons (Andermann et al., 2002; Cornell and Eisen, 2002); in its absence, cells differentiate as myelinating Schwann cells (McGraw et al., 2008). Although Neurog transcription factors clearly determine sensory neuron identity, the mechanism by which their expression is initiated is unclear.

To identify genes implicated in the initial cell fate decisions in DRG, we conducted a mutant screen in the zebrafish for mutants lacking DRG sensory neurons. We isolated a mutant, *sensory deprived* (*sdp*), in which neural crest derivatives form normally with the exception of the DRG. Subsequent work mapped the associated mutation to the gene encoding Reck (reversion-inducing, cysteine-rich protein containing Kazal motifs), an inhibitor of metalloproteinases (Takahashi et al., 1998). *reck* has previously been implicated in the development of the mammalian cortex (Muraguchi et al., 2007) and circulatory system (Oh et al., 2001). In cell culture studies, loss of *reck* function is associated with a hypermigratory phenotype (Morioka et al., 2009; Silveira Corrêa et al., 2010), presumably because upregulated metalloproteinase activity allows cells to permeate the extracellular matrix more easily. This cell migratory behavior is reflected in studies of human cancers, which are more aggressive following Reck inactivation (Clark et al., 2007). Our results suggest a mechanistic link between termination of migration and initial differentiation of sensory neuron precursors from the neural crest.

[1]Graduate Program in Neurobiology and Behavior, [2]Molecular and Cellular Biology Graduate Program, [3]Department of Biological Structure, University of Washington, Seattle, WA 98195-7420, USA. [4]Program in Genomics of Differentiation, National Institute of Child Health and Human Development, National Institutes of Health, 6B/3B309, Bethesda, MD 20892, USA.

*Author for correspondence (draible@u.washington.edu)

Accepted 11 January 2012

MATERIALS AND METHODS

Zebrafish husbandry

Zebrafish were maintained at 28.5°C on a 14-hour/10-hour light/dark cycle following established methods and Institutional Animal Care and Use Committee standards (Westerfield, 2007). Embryos were maintained in E2 medium, and staged according to Kimmel et al. (Kimmel et al., 1995). DRG were identified using Tg(*neurog1:egfp*)^{w61} (McGraw et al., 2008).

Transgenic lines

The 4.9 kb *sox10* promoter (Carney et al., 2006), fluorescent protein Eos (Wiedenmann et al., 2004) (Evrogen) or nls-Eos, and a polyadenylation sequence (Kwan et al., 2007) were Gateway cloned (Invitrogen) to generate pSox10:Eos/pSox10nls-Eos; clones were microinjected with Tol2 transposase to generate germline transgenics *Tg(sox10:eos)*^{w9} and *Tg(sox10:nlseos)*^{w18} as previously described (Fisher et al., 2006).

Immunohistochemistry

Embryos were stained with the antibodies mouse anti-Elavl1 (Invitrogen), 1:500; rabbit anti-GFP (Invitrogen) 1:1000; mouse anti-acetylated tubulin (Sigma; 1:5000), mouse anti-MF20 (Developmental Studies Hybridoma Bank, University of Iowa; 1:100), rabbit anti-Sox10 (gift of Sarah Kucenas, University of Virginia; 1:500), as previously described (Ungos et al., 2003) and imaged by confocal microscopy.

Genetic screen

We treated *AB males with 3 mM ethylnitrosourea (Solnica-Krezel et al., 1994). F_3 progeny were screened by immunostaining for Elavl1. *Sdp*^{w15} was identified in the *AB background during screening. Three additional alleles were identified: *sdp*^{w13} by complementation screening against *sdp*^{w15} carriers and *sdp*^{w12} and *sdp*^{w14} isolated as novel mutations and later established as *sdp* alleles by complementation.

Mutation identification

sdp^{w12} heterozygotes were outcrossed to the Wik strain and F_2 progeny were subjected to bulked segregant analysis using SSLP markers followed by analysis of individuals, as described (Bahary et al., 2004). Zebrafish *reck* sequence was generated by alignment of expressed sequence tags (ESTs) identified by BLAST search using *Mus musculus* RECK protein as the search string, and used as a template to clone the zebrafish cDNA by PCR. Staged embryos were homogenized in Trizol (Invitrogen), and total RNA was isolated by column purification (Qiagen). RNA was treated with DNAse I (Fermentas) to remove genomic DNA and reverse transcribed (Invitrogen). Amplicons were cloned into pCR4-TOPO (Invitrogen) and sequenced.

To identify *sdp*^{w12} mutant embryos, tissue was homogenized by overnight incubation in 200 μg/μl proteinase K. A 233 bp amplicon was PCR-amplified from genomic DNA using primers (F: 5′-GAATCTCCACCCA-TCGCCAAGATG-3′; R: 5′-GAATGTTAGCAGCTGTGAGGTTTG-3′) and digested with *Ava*II (NEB), which cuts the wild-type product.

Morpholino oligonucleotide knockdown

A splice-blocking morpholino oligonucleotide (MO) with the sequence CAGGTAGCAGCCGTCACTCACTCTC was generated based on prediction of efficacy by the manufacturer (Gene Tools). This MO targets the *reck* exon 7-intron 7 boundary. Injected embryos were processed for cDNA as above. We designed primers flanking intron 7 (F: 5′-CATCAACAACTCACTACCAGGAGC-3′, exon 7; R: 5′-GGGTGTA-GTCTGGTGTAGTTCTCC-3′, exon 8) to detect appropriately spliced *reck* transcript.

Angiograms

Tg(fli1a:egfp)^{y1} embryos (Lawson and Weinstein, 2002) were injected at 48 hours post-fertilization (hpf) in the sinus venosus with a 40% solution of Qdot fluorescent nanocrystals (Invitrogen) as previously described (Kamei et al., 2010; Weinstein et al., 1995) and imaged using an Olympus FluoView FV-1000 confocal microscope.

mRNA injection

Wild-type (*wt*) and *sdp*^{w12} *reck* coding sequences were ligated into pCS2p+, linearized with *Not*I and transcribed in vitro with SP6 polymerase to generate capped, polyadenylated mRNA (Ambion). A range of mRNA concentrations was injected into embryos derived from a cross between *Tg(neurog1:egfp)/sdp*$^{w12/+}$ parents. Data were analyzed using a two-factor ANOVA; post-hoc significance between conditions was determined using the Scheffé method.

In situ hybridization

Digoxigenin-labeled riboprobes for *crestin* (Rubinstein et al., 2000) and *neurog1* (Korzh et al., 1998) were generated as previously described. A 2.1 kb fragment of *reck* was subcloned into pBluescript II SK, linearized with *Eco*RV and transcribed with T7 polymerase (Invitrogen) to generate digoxigenin-labeled riboprobe. In situ hybridization was carried out as previously described (Thisse and Thisse, 2008). Fluorescent in situ hybridization was carried out as previously described (Vize et al., 2009). Embryos were then embedded in 4% agarose and sectioned at 100 μm on a Leica VT1000S vibratome. Colocalization of *reck* and *crestin* was analyzed by confocal imaging in single optical planes sampled every 7 μm. The anterior-posterior position of each section was determined by alignment to the section containing the yolk constriction.

Metalloproteinase activity

Tg(neurog1:egfp)/sdp$^{w12/+}$ parents were incrossed; the resulting embryos were sorted by phenotype at 48 hpf and homogenized in lysis buffer (150 mM NaCl, 10 mM HEPES, 2 mM DTT, 0.1% Triton X-100, pH 8.0). Protein concentration was normalized using the Bradford method. Lysate was incubated with DQ gelatin (Invitrogen) at room temperature; fluorescence was assayed using a fluorimeter (Tecan).

Transplants

Donor *Tg(neurog1:egfp)* embryos were injected with 1 nl 2.5% tetramethyl rhodamine dextran, 0.1 M KCl and either 1.75 μg/μl *reck* MO or sterile water. Host *nacre*$^{w2/w2}$ embryos were injected at the one-cell stage with 1 nl 0.2% Phenol Red, 0.1 M KCl and either 1.75 μg/μl *reck* MO or sterile water. Donor and host embryos were dechorionated and mounted in 4% methylcellulose at sphere or dome stage (~3.5-4.5 hpf). Cells were aspirated into a pulled capillary glass needle and deposited into host embryos. Transplants were allowed to recover in E2 media supplemented with 100 U penicillin/100 μg/ml streptomycin.

Neural crest migration measurements

Tg(sox10:eos)/sdp$^{w12/+}$ fish were incrossed; the resulting clutch was fixed at 24 hpf, immunostained for MF20 and imaged by confocal microscopy. A threshold was applied to the images using Photoshop and images were then subjected to a MatLab (Mathworks) algorithm measuring the length of *y*-direction signal (i.e. first black pixel to last black pixel) for each *x* coordinate. This plot was smoothed by averaging over 10-point bins. Local maxima were detected by an iterative point-to-point comparison function (peakdet, http://billauer.co.il/peakdet.html).

Time-lapse microscopy and cell tracking

Tg(sox10:nls-eos) embryos (18 somite-stage; 18s) and *Tg(sox10:nls-eos)/Tg(neurod:tagrfp)*^{w69} embryos (30 hpf) were immobilized in 1.5% Type VII agarose (Sigma) and imaged every 10 minutes using a 3i Marianas spinning disk confocal microscope system. Image files were processed using Slidebook (3i) and ImageJ (NIH) software. Movies from the early interval were initiated at the beginning of neural crest migration. Movies from the late interval were synchronized so that the lateral line crosses somite 16 at the same frame. Divisions were identified by resolution of mitotic figures; cell death was determined by nuclear fragmentation.

Cell tracking was performed manually in ImageJ. Dorsoventral cell velocity was defined as the sum of *y*-axis displacements divided by the number of frames in which the cell was visible. Proliferative and apoptotic rates were defined by the following equation:

$$\left(\frac{x}{n_{cells} \times t_{frames}}\right) \times 144 , \quad (1)$$

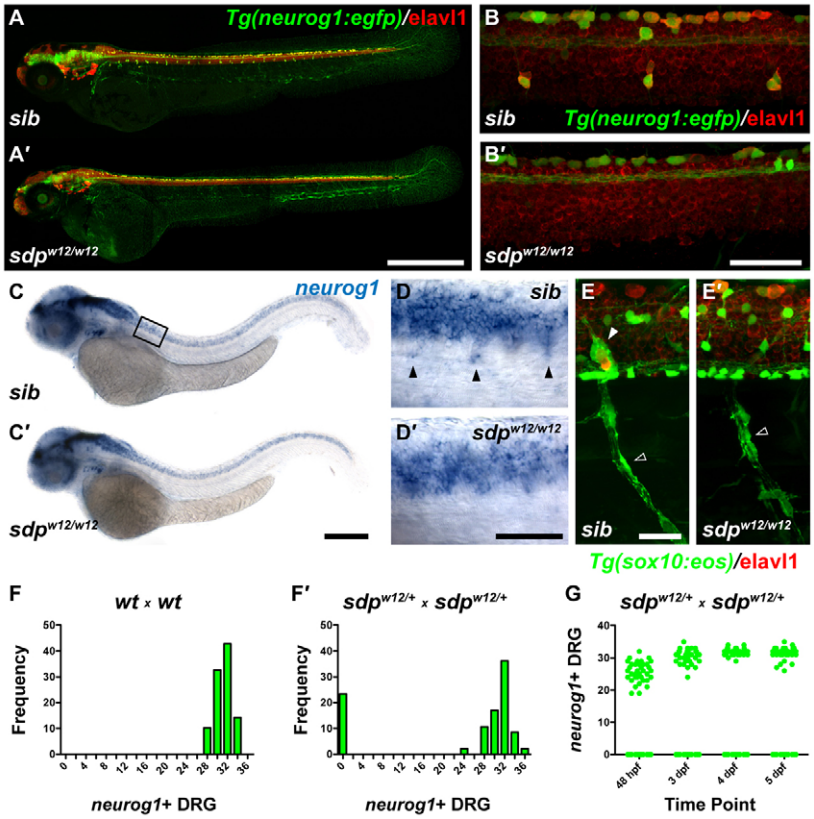

Fig. 1. *sensory-deprived* (*sdp*) mutants exhibit a complete loss of DRG sensory neurons. (**A**) *Tg(neurog1:egfp)* zebrafish embryos (3 dpf) immunostained for Elavl1. (**A′**) DRG are absent in an *sdp*$^{w12/w12}$ mutant embryo. Scale bar: 500 μm. (**B**,**B′**) High magnification images of A and A′. Scale bar: 50 μm. (**C**,**C′**) *neurog1* expression at 48 hpf. Box indicates position of high magnification images in D,D′. Scale bar: 250 μm. (**D**,**D′**) High magnification image of C and C′. Scale bar: 50 μm. Arrowheads indicate neurog^{+} DRG sensory neuron precursors. (**E**,**E′**) *Tg(sox10:eos)* embryo (3 dpf) immunostained for Elavl1. Although Schwann glia (empty arrowhead) are retained, satellite glia (filled arrowhead) are absent in *sdp*$^{w12/w12}$. Scale bar: 25 μm. (**F**,**F′**) Counts of *neurog1*$^{+}$ DRG at 3 dpf. Approximately 25% of embryos fail to form DRG, suggesting that *sdp*^{w12} is a fully penetrant recessive mutation. (**G**) Counts of *neurog1*$^{+}$ DRG followed over four days. DRG never appear in ~25% of the population, indicating that *sdp* does not delay in DRG development.

where x is the number of events observed per time lapse, n_{cells} is the total number of cells tracked and t_{frames} is the number of frames (each separated by 10 minutes). Multiplying by 144 yielded the number of events per cell-day.

Drug experiments

Tg(neurog1:egfp)/sdp^{w12} embryos were treated in drug dissolved in 1% DMSO in E2 medium from 16s to 3 days post-fertilization (dpf); drug solution was changed daily. Embryos were fixed and immunostained for Elavl1 and GFP. Drugs were administered at the following concentrations: GM6001 (Enzi Life Sciences), 100 μM; batimastat (Tocris Biosciences), 500 μM; marimastat (Tocris Biosciences), 100 μM; DAPT (Sigma), 100 μM.

TUNEL staining

Fish were fixed at 30 hpf and immunostained with rabbit anti-Sox10 antibody. Embryos were permeabilized with 20 μg/ml proteinase K (Sigma) and subjected to TUNEL labeling using fluorescein substrate (Roche). TUNEL^{+} and Sox10^{+} cells were counted from confocal stacks and the embryos were subsequently genotyped.

RESULTS

sdp is a recessive phenotype involving the loss of DRG neurons

To identify mutations that alter DRG development, we screened for perturbed expression of Elavl1 in the peripheral nervous system (Henion et al., 1996; Marusich et al., 1994; Szabo et al., 1991). We identified four alleles of a recessive mutation, *sensory deprived* (*sdp*). All mutant embryos completely lack DRG up to and including 5 dpf (Fig. 1, supplementary material Fig. S1). However, for all mutations all other neural crest derivatives appear to develop normally (supplementary material Fig. S2), including pigment cells, enteric neurons, lateral line glia and sympathetic chain (supplementary material Fig. S2); although normal in morphology, the ceratohyal cartilage is displaced (supplementary material Fig. S2K-L′). Cranial ganglia, which have both neural crest and placode origin, appear normal (supplementary material Fig. S2) and have comparable cell counts (supplementary material Fig. S3). Fish homozygous for any of the *sdp* alleles die by day 12.

Mutant embryos display defects in DRG formation at the earliest stages of their development. *sdp* embryos exhibit no *neurog1* expression in DRG precursors as assessed by a *neurog1:egfp* transgenic line (Fig. 1A-B′) and by in situ hybridization for *neurog1* transcript (Fig. 1C-D′). In addition, no cells in the periphery ectopically express these markers, nor are any ectopic neurons revealed by Elavl1 staining, suggesting that the *sdp* phenotype is not caused by DRG displacement. By contrast, *neurog1* expression in the central nervous system and cranial placodes appears normal. These results suggest that the *sdp* phenotype is a result of a defect occurring upstream of *neurog1*.

Neurons and glia of the zebrafish DRG are derived from a common subpopulation of neural crest (Raible and Eisen, 1994; McGraw et al., 2008). The *sdp* phenotype could be caused by a failure to specify this neuroglial lineage or by a later defect in neuronal differentiation. To address this question, we generated the transgenic line *Tg(sox10:eos)*, in which the fluorophore Eos (Wiedenmann et al., 2004) is expressed under the control of the promoter for *sox10*, an SRY box-containing transcription factor expressed in neural crest and maintained in crest-derived glial cells (Carney et al., 2006). Schwann cells apposed to motor axons are retained in *sdp* embryos; however, satellite glia adjacent to DRG are notably absent (Fig. 1E,E′). Schwann cells are also found to be normally distributed along the lateral line nerve (supplementary material Fig. S2E,H). We conclude that in *sdp* mutants DRG neuron formation is compromised rather than specification of the neuroglial lineage.

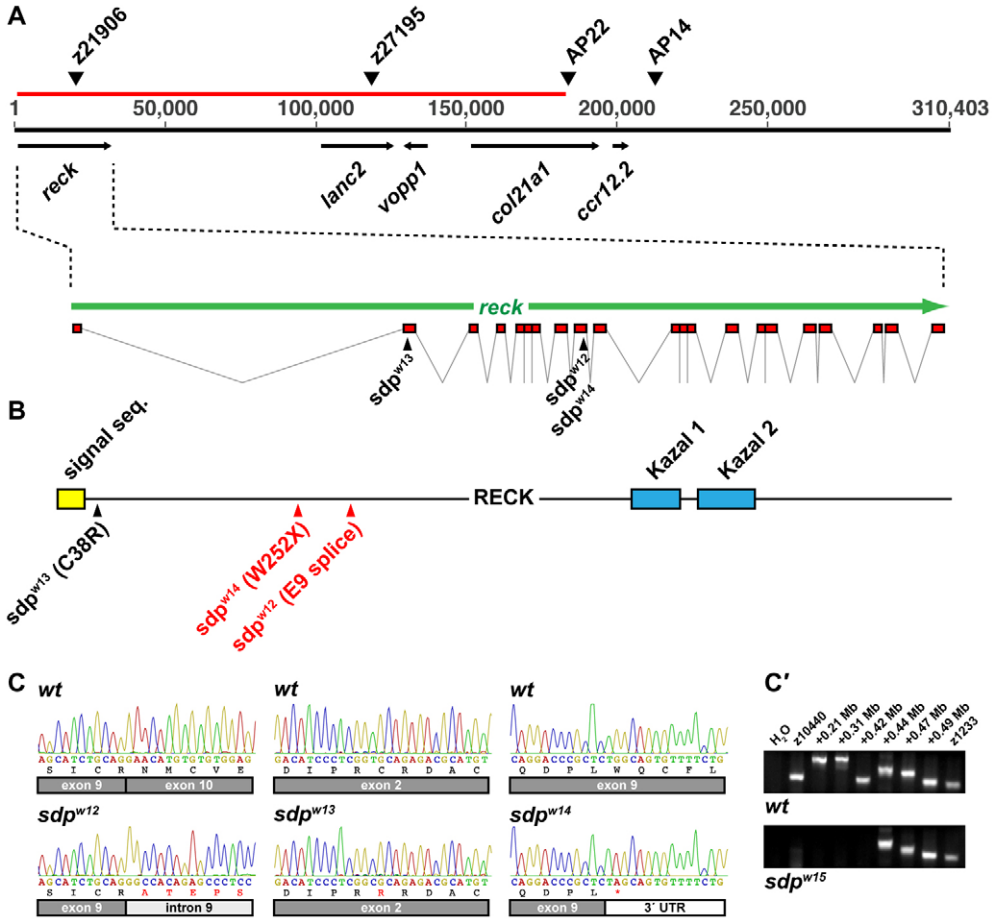

Fig. 2. *sdp* alleles exhibit lesions in the *reck* coding sequence. (**A**) Physical map of the end of chromosome 24. *sdp* critical region (red line) contained at least four genes; simple sequence length polymorphism (SSLP) markers used for mapping are shown and locations of lesions indicated. (**B**) Predicted protein product zebrafish *reck* is 956 amino acids long and has an N-terminal signal sequence and two Kazal motifs. (**C**) Electropherograms showing each of the *reck* single nucleotide polymorphisms (SNPs). sdp^{w12} is a splice site mutation at the exon 9-intron 9 boundary, sdp^{w13} is a C38R substitution in exon 2, sdp^{w14} is a W252X substitution in exon 9. (**C′**) sdp^{w15} is a large deletion of chromosome 24 encompassing at least 0.4 Mb and including the entire *sdp* critical region.

All *sdp* alleles have sequence polymorphisms in the *reck* gene

To identify the genomic location of *sdp* alleles, we used recombination mapping in an sdp^{w12}/Wik hybrid background. We identified a critical region of ~200 kb on chromosome 24 associated with *sdp* (Fig. 2A). Direct sequencing of sdp^{w12} cDNA corresponding to transcripts in this region identified a mutation in the exon 9 splice donor of *reck* that caused a 510 bp intron to be retained (Fig. 2C). This intron contains a stop codon, which would truncate any translated protein to 309 amino acids. *reck* encodes a 956 amino acid protein containing an N-terminal signal sequence and two Kazal motifs (Fig. 2B); it is a glycosylphosphatidylinositol (GPI)-linked inhibitor of metalloproteinases (Takahashi et al., 1998). All *sdp* alleles possessed perturbations in the *reck* sequence (Fig. 2B-C′): a C38R missense mutation in a highly conserved residue (sdp^{w13}), a W252X premature stop mutation (sdp^{w14}) and a 0.5 Mb deletion of chromosome 24 that eliminates at least four other genes in addition to *reck* (sdp^{w15}). Although each *sdp* allele possesses a different lesion in *reck*, they are equivalent with respect to the DRG phenotype (supplementary material Fig. S1). Complementation analysis reveals that *w12*, *w13* and *w14* are likely to be null alleles as no additional phenotypes were observed when crossed to the *w15* deficiency (not shown). The severe swelling phenotype of the *w15* deficiency (supplementary material Fig. S1) is reduced by complementation, suggesting that this phenotype is affected by loss of additional genes found in the interval.

Metalloproteinases are upregulated in *sdp* embryos

Reck inhibits the maturation and activity of the metalloproteinases Mmp2, Mmp9, Mmp14 and Adam10 (Muraguchi et al., 2007; Oh et al., 2001; Takahashi et al., 1998). We incubated protein extracts from 48 hpf $sdp^{w12/w12}$ and sibling embryos with a fluorescein/gelatin conjugate, and found that mutant embryos exhibited greater metalloproteinase activity than siblings (supplementary material Fig. S4). Reck therefore appears to be a major inhibitor of metalloproteinases in developing zebrafish embryos.

Morpholino oligonucleotide knockdown of *reck* transcript phenocopies the DRG phenotype observed in *sdp*

To confirm that *reck* loss of function is the cause of the DRG phenotype observed in *sdp*, we generated a splice-blocking MO directed against the exon7-intron7 boundary. Embryos injected with this MO fail to develop DRG (Fig. 3A-D) despite the appropriate formation of cranial ganglia (Fig. 3C), Schwann cells (Fig. 3G), lateral line glia (Fig. 3H) and pigment cells (Fig. 3I), matching the phenotypes of *reck* mutants. DRG counts declined in a dose-dependent fashion (Fig. 3E). We verified that *reck* expression was disrupted by this MO by subjecting cDNA to quantitative RT-PCR using primers flanking intron 7 (Fig. 3F). These primers generate an amplicon of 366 bp when applied to appropriately spliced transcript; we cannot detect this amplicon

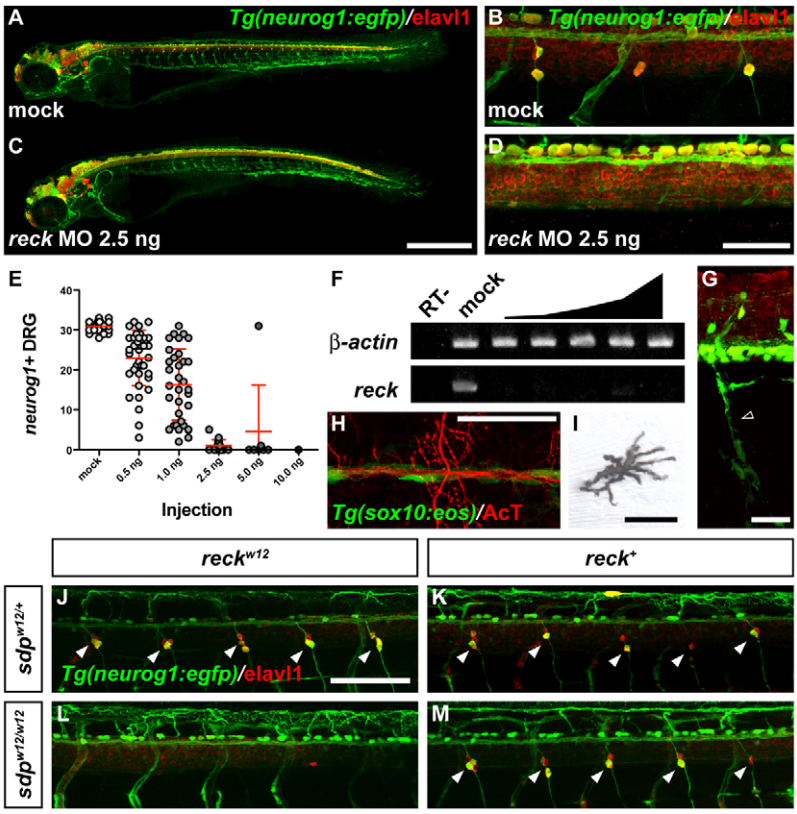

Fig. 3. Phenocopy of *sdp* with *reck* MO and rescue by expression of wild-type *reck*. (**A-D**) Mock injected (A,B) and MO-injected (C,D) 3 dpf *Tg(neurog1:egfp)* embryos immunostained for Elavl1. Scale bar: 500 μm in A,C; 50 μm in B,D. (**E**) *neurog1*$^{+}$ DRG at 3 dpf in embryos injected with indicated doses of *reck* MO. Error bars represent s.d. (**F**) Loss of correctly spliced *reck* transcript with *reck* MO. RT–, negative control reaction without reverse transcriptase. (**G-I**) *Tg(sox10:eos)* embryo (3 dpf) injected with 1.5 ng *reck* MO and immunostained for Elavl1. (G) Crest-derived Schwann glia (empty arrowhead) are retained. Scale bar: 25 μm. (H) Crest-derived lateral line glia are retained. Scale bar: 50 μm. (I) Crest-derived pigment cells (melanophore shown) are retained. Scale bar: 25 μm. (**J-M**) Injection of 200 pg *sdp*^{w12} *reck* mRNA has no effect on *sdp*$^{w12/+}$ (J) or *sdp*$^{w12/w12}$ (L) fish. Injection of *wt reck* mRNA has no effect on *sdp*$^{w12/+}$ fish (K) but rescues DRG formation in *sdp*$^{w12/w12}$ fish (M). Scale bar: 100 μm. Arrowheads indicate DRG neurons.

in cDNA from embryos injected with *reck* MO. These results confirm that DRG formation fails in the absence of *reck* function.

Expression of *reck* rescues DRG in *sdp* embryos

To show that reintroduction of *reck* was sufficient to rescue the *sdp* phenotype, we injected *wt* or *sdp*^{w12} mutant mRNA into embryos derived from *sdp*$^{w12/+}$ incrosses (Fig. 3, Table 1). Injection of mutant mRNA has no effect on mutants or siblings (Fig. 3J,L). Injection of *wt reck* mRNA restores DRG to wild-type levels in *sdp*$^{w12/w12}$ embryos (Fig. 3M). Overexpression of *wt reck* mRNA fails to generate any observable phenotype on its own (Fig. 3K). We conclude that *reck* loss of function is solely responsible for the DRG defect observed in *sdp*.

Expression of *reck* is consistent with a role in the development of neural crest derivatives

We examined *reck* expression by in situ hybridization to identify tissues in which *reck* might act to influence DRG development. In situ hybridization for *crestin* was used to identify neural crest. In the trunk, *crestin* is expressed adjacent to the dorsal neural tube and in cells migrating between neural tube and somite (Fig. 4A,B, supplementary material Fig. S5C,D,I-I‴), whereas *reck* is expressed primarily in ventral mesoderm, consistent with a role in vasculature development (Fig. 4A,B, supplementary material Fig. S5G,H,J-J‴). However, a band of dorsal *reck* expression appears at 22 hpf (Fig. 4A,B, supplementary material Fig. S5G,H,J-J‴). This dorsal expression is transient, disappearing by 30 hpf (Fig. 4C,D)

To quantify the degree to which *reck* and *crestin* expression colocalize, embryos at 22 and 30 hpf were subjected to double fluorescent in situ hybridization followed by serial sectioning (Fig. 4B,D). Cells were counted as *reck*$^{+}$, *crestin*$^{+}$ or *reck/crestin*$^{+}$ in each section. At 22 hpf, essentially all neural crest cells express *reck*. Although fewer neural crest cells are observed in posterior segments, we do not observe significant changes in *reck/crestin* colocalization (Fig. 4E,G). By 30 hpf, however, the expression of *reck* and *crestin* has largely separated into two separate cell populations (Fig. 4F,G); however, a small subset of cells (about three cells per hemisegment) continues to express both *reck* and *crestin*.

Table 1. Injection of *reck* mRNA rescues *sdp*$^{w12/w12}$ in a dose-dependent fashion

			Dorsal root ganglia			
Genotype	Injection	Dose	Mean	s.d.	*n*	*P*
+/+	Mock	–	29.6	1.6	8	–
	wt	100 pg	27.9	3.4	8	n.s.
		200 pg	29.8	2.6	4	n.s.
	sdp^{w12}	100 pg	31.1	1.4	9	n.s.
		200 pg	30.3	1.6	8	n.s.
+/w12	Mock	–	29.9	2.3	30	–
	wt	100 pg	27.7	3.0	19	n.s.
		200 pg	27.7	4.5	9	n.s.
	sdp^{w12}	100 pg	31.1	2.6	16	n.s.
		200 pg	30.2	2.0	22	n.s.
w12/w12	Mock	–	0.0	0.0	10	–
	wt	100 pg	15.4	8.8	10	<0.001
		200 pg	23.4	2.9	5	<0.001
	sdp^{w12}	100 pg	0.0	0.0	10	n.s.
		200 pg	0.0	0.0	2	n.s.

DRG counts of mRNA-injected embryos at 4 dpf are displayed with s.d. for each genotype/injection permutation. A two-way analysis of variance showed that the injection factor was significant, F(4,155)=19.77, *P*=3.61E-13. The Scheffé post-hoc criterion for significance revealed that only the injection of *wt reck* into *sdp*$^{w12/w12}$ embryos had a significant effect on DRG counts relative to mock-injected embryos of the same genotype (100 pg, 15.4±8.8; 200 pg, 23.4±2.9; mean±s.d.).

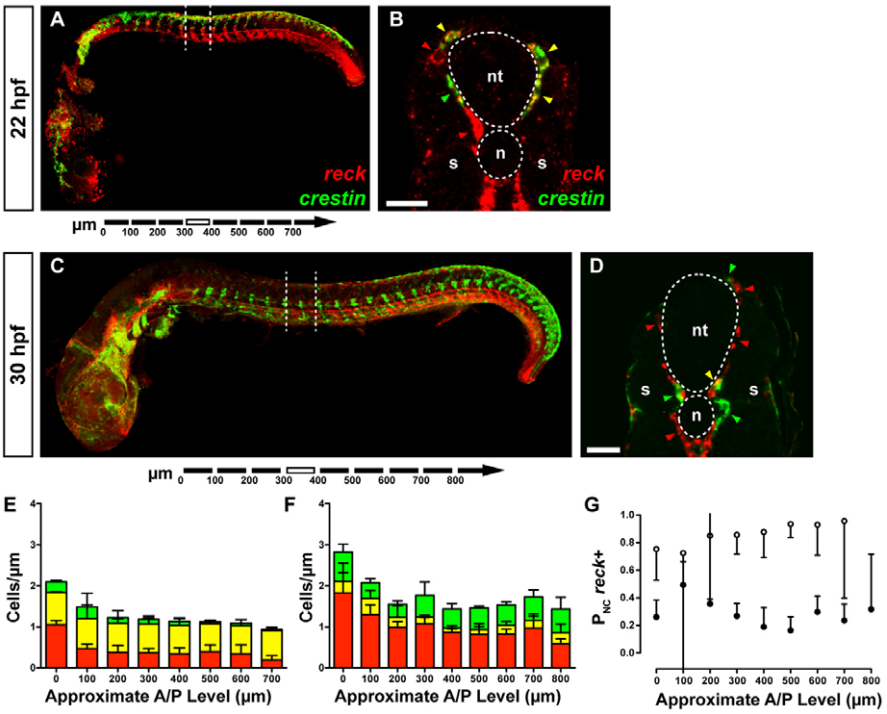

Fig. 4. *reck* expression in neural crest cells. (**A**) Whole-mount zebrafish embryo (22 hpf). Dashed lines indicate the plane of section shown in B. (**B**) *reck*$^+$ cells (red arrowheads) are present in both the developing vasculature and presumptive neural crest. A small number of *crestin*$^+$ cells are also visible (green arrowhead). Most *crestin*$^+$ cells are also *reck*$^+$ (yellow arrowheads). Scale bar: 25 μm. (**C**) Whole-mount embryo (30 hpf). Dashed lines indicate the plane of the section shown in D. (**D**) Many *reck*$^+$ cells (red arrowheads) are present in the developing vasculature. Many *crestin*$^+$ cells (green arrowheads) are now apparent with few *crestin*$^+$/*reck*$^+$ cells (yellow arrowhead), suggesting the two markers have resolved into different populations. Scale bar: 25 μm. (**E**,**F**) Cell counts from serial sections of 22 hpf (E) and 30 hpf (F) embryos. Error bars represent s.d. Green, *crestin*$^+$ cells; yellow, *crestin*$^+$/*reck*$^+$ cells; red, *reck*$^+$ cells. (**G**) *crestin*$^+$/*reck*$^+$ cells as a proportion of all cells expressing *crestin* for 22 hpf (white circles) and 30 hpf (black circles) embryos. In most segments we observe significant segregation of *crestin* and *reck* expression. Error bars represent 95% confidence interval. n, notochord; nt, neural tube; s, somite.

MO-injected embryos exhibit vasculature defects

Mice with a targeted disruption of the *reck* locus display impaired vascular maturation and abdominal hemorrhage (Oh et al., 2001). To determine whether *reck*-deficient zebrafish embryos exhibit similar defects, we injected *reck* MO into *Tg(fli1a:egfp)* embryos, a transgenic reporter expressed in the endothelial cells of the vasculature (Lawson and Weinstein, 2002). Between 24 and 32 hpf, vasculature in MO-injected embryos is comparable to the vasculature of control embryos, although slightly delayed (Fig. 5A-C,G-I, supplementary material Table S1). However, by 48 hpf, moderate defects in circulation and vascular development are manifest. The parachordal vessel (PAV), a derivative of the caudal vein, often fails to form following *reck* knockdown (Fig. 5D,J, supplementary material Table S1). Additionally, although circulation initiates normally in MO-injected embryos, angiograms reveal poor perfusion in intersegmental vessels (Fig. 5E,K) as well as significantly impaired axial circulation (supplementary material Table S1). At 3 dpf, intracranial hemorrhage is apparent in *reck*-deficient embryos, suggesting that vascular integrity is also impaired (Fig. 5F,L, supplementary material Table S1). These results demonstrate that, as in mouse, loss of *reck* is associated with disruption of vasculature development.

The requirement for *reck* in DRG development is cell autonomous

Previous work has demonstrated that Reck is a GPI-linked protein that inhibits metalloproteinases in cis, blocking activity in the cell in which it is expressed (Muraguchi et al., 2007). *reck* is expressed in both neural crest and the environment through which it migrates, including vascular precursors that themselves have defective development. Therefore, the failure of DRG to form in the absence of *reck* function could be attributed either to cell environment or to incompetence in the neural crest itself. To differentiate between these possibilities, we performed transplants between MO- and mock-injected embryos.

Donor cells were derived from rhodamine-labeled *Tg(neurog1:egfp)* embryos and transplanted into *nacre* (*mitfa* – Zebrafish Information Network) host embryos (Lister et al., 1999); the resulting transplants were then immunostained for Elavl1. This allowed us to identify all donor cells incorporated into the transplant (rhodamine), donor cells which differentiated into sensory neurons (GFP), and all differentiated neurons in the transplant (Elavl1). Because *nacre* embryos lack trunk melanophores, we were able to verify whether donor cells had become neural crest by the appearance of donor-derived melanophores. Analysis was restricted to those embryos in which melanophores developed.

When cells from mock-injected embryos are deposited into mock-injected hosts, they are able to differentiate into DRG sensory neurons (Fig. 6A,B, Table 2). However, when cells from MO-injected embryos are transplanted into mock-injected embryos, they never form DRG neurons, despite the fact that donor cells frequently generate neural crest (Fig. 6C,D). Conversely, when cells from mock-injected donors are transplanted into MO-injected hosts, they form DRG neurons readily but are unable to induce host cells to form DRG neurons (Fig. 6E,F). Therefore, we conclude that *reck* is required cell autonomously in migrating neural crest for normal DRG formation.

Altered neural crest migration after perturbation of *reck*

Prior work has established that suppression of *reck* function leads to hypermigratory behavior in several cell lines (Chang et al., 2006; Liu et al., 2003; Morioka et al., 2009; Yoshida et al., 2008); conversely, forced expression of *reck* reduces migration (Hsu et al., 2006; Kang et al., 2007; Liu et al., 2003; Morioka et al., 2009; Silveira Corrêa et al., 2010; Yoshida et al., 2008). We hypothesized that *reck* loss of function might cause the neural crest to migrate excessively, causing the DRG deficit observed in *sdp*. We first measured the dorsoventral migration of neural crest streams at 24

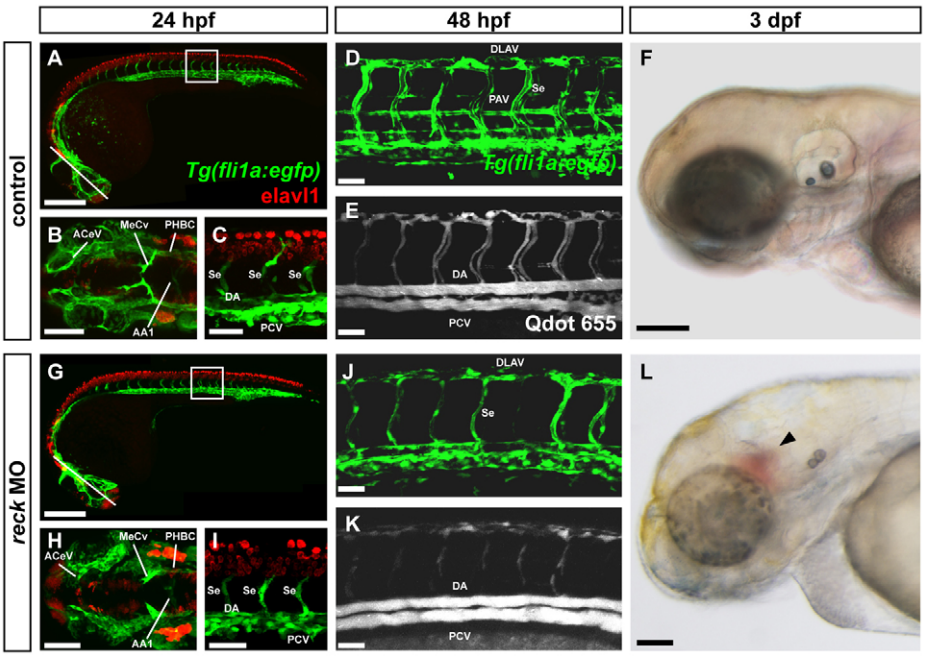

Fig. 5. *reck*-deficient embryos exhibit defects in vascularization. Mock-injected (A-F) and *reck* MO-injected (G-L) zebrafish embryos. (**A**,**G**) *Tg(fli1a:egfp)* zebrafish embryo (24 hpf) immunostained for Elavl1. Line indicates plane of image in B,H; box indicates area of image in C,I. Scale bars: 250 μm. (**B**,**H**) Cranial vasculature. AA1, mandibular arch; ACeV, anterior cerebral vein; MeCV, middle cerebral vein; PHBC, primordial hindbrain channel. Scale bars: 100 μm. (**C**,**I**) Trunk vasculature. DA, dorsal aorta; PCV, posterior cardinal vein; Se, intersegmental vessel. Scale bars: 50 μm. All blood vessels form normally in MO-injected animals but are slightly delayed in their extension. (**D**,**J**) *Tg(fli1a:egfp)* embryo (48 hpf). DLAV, dorsal longitudinal anastomotic vessel; PAV, parachordal vessel. The PAV is reduced in size or fails to form entirely in MO-injected embryos. Scale bars: 50 μm. (**E**,**K**) Qdot angiogram of the embryo shown in D,J. Although blood flows through the DA and PCV after MO injection, blood flow is somewhat reduced in the DLAV and intersegmental vessels. Scale bars: 50 μm. (**F**,**L**) Brightfield image of 3 dpf embryo. Cranial hemorrhage (arrowhead) is visible in a significant fraction of MO-injected embryos. Scale bars: 135 μm.

hpf and found no significant difference in neural crest migration distance (supplementary material Fig. S6), suggesting that the overall extent of migration is not perturbed.

We next used time-lapse microscopy to search for more subtle differences in neural crest behavior at two different stages of development. We first imaged *Tg(sox10:nls-eos)* embryos between 18s and 30 hpf; this interval encompasses initiation of neural crest migration (Fig. 7A-F, supplementary material Movies 1, 2). Movies were analyzed as the first neural crest cell began to migrate ventrally. The position of each *sox10*$^{+}$ cell was manually tracked and its velocity in the dorsoventral axis was measured. We also followed cell count, proliferation and apoptosis. During the initial migration of neural crest, we found cell velocity to be ~40% faster in *reck*-depleted neural crest cells (2.66±0.25 μm/10 minutes, n=40 cells versus 1.88±0.24 μm/10 minutes, n=54 cells; mean ± s.e.m., P=0.028). The overall number of cells, the rate of proliferation and the rate of apoptosis are unchanged over this interval (Fig. 7C-F).

To examine migratory behavior in differentiating neural crest cells, we imaged uninjected and *reck* MO-injected *Tg(sox10:nls-eos)/Tg(neurod:tagrfp)* embryos between 30 and 60 hpf; this interval includes the overt expression of the first neuronal markers in DRG sensory neurons (Fig. 7G-L, supplementary material Movies 3, 4). The position of each *sox10*$^{+}$ cell was manually tracked, and velocity (Fig. 7J), cell count (Fig. 7I), proliferation (Fig. 7K) and apoptosis (Fig. 7L) were measured as above. At this stage, we found cell velocity of *reck*-depleted neural crest cells to be half that of control cells (0.54±0.03 μm/10 minutes, n=72 cells versus 1.14±0.14 μm/10 minutes, n=163 cells; mean ± s.e.m., P=0.005). The rate of proliferation and the overall number of cells are not statistically different following *reck* depletion. We observed a small but significantly greater apoptotic rate in *reck*-depleted neural crest cells compared with that in uninjected embryos, although still too infrequent to significantly change overall cell number.

To determine whether neural crest cells are capable of inhabiting the appropriate microenvironment for DRG formation following *reck* depletion, we assessed the dorsoventral position of each cell at each time point (Fig. 7M). DRG precursors were previously noted to perform a dorsalward migration to the position of the future ganglion prior to differentiation (Raible and Eisen, 1994). This dorsal migration corresponds to the initiation of *neurog1* expression (McGraw et al., 2008). We found that by 55 hours, 68% of crest-derived *sox10*$^{+}$ cells observed in uninjected embryos are situated in this microenvironment, compared with only 20% in MO-injected embryos (Fig. 7M). Therefore, in the absence of *reck*, neural crest cells exhibit aberrant migratory behavior and fail to inhabit the appropriate position for differentiation into DRG.

DISCUSSION

The developmental phenotypes observed in our *reck* alleles reflect, in part, those seen in a previously published mouse knockout model (Oh et al., 2001). *reck* is expressed in the zebrafish vasculature up to and including 48 hpf (data not shown). We observe no overall gross deficit in trunk vasculogenesis; however, the parachordal chain fails to form in *reck*-deficient embryos. Additionally, *reck* MO-injected embryos exhibit hypoperfusion and

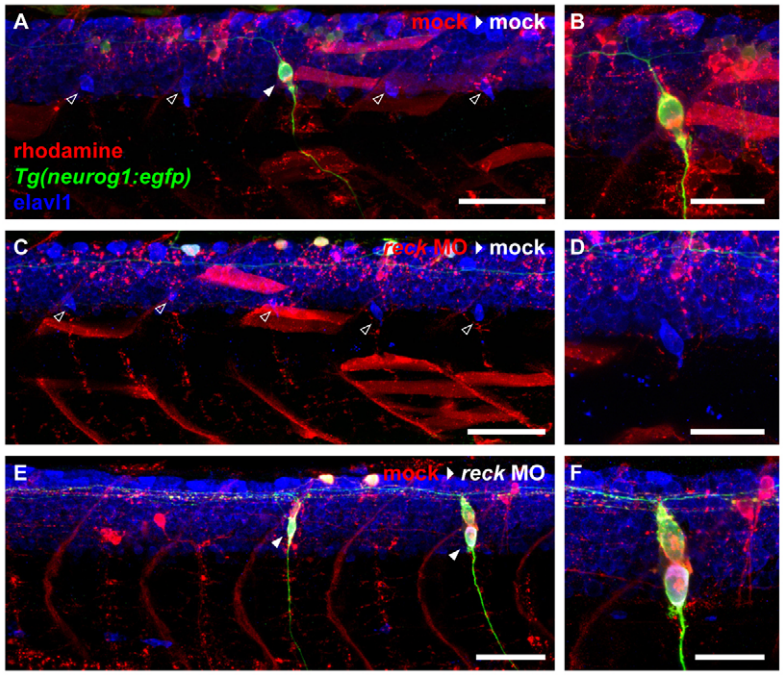

Fig. 6. DRG defects from *reck* depletion are cell-autonomous. (**A**) Mock-injected zebrafish embryo (3 dpf) implanted with mock-injected cells. Four host-derived DRG are visible (empty arrowheads) flanking one donor-derived DRG (filled arrowhead). Scale bar: 50 μm. (**B**) High magnification image of the donor-derived DRG shown in A. Scale bar: 25 μm. (**C**) Mock-injected embryo (3 dpf) implanted with MO-injected cells. Five host-derived DRG are visible (empty arrowheads), but donor cells never give rise to DRG. Scale bar: 50 μm. (**D**) High magnification image of one of the host-derived DRG shown in C. Scale bar: 25 μm. (**E**) MO-injected embryo (3 dpf) implanted with mock-injected cells. Only donor-derived DRG (filled arrowheads) are present. Scale bar: 50 μm. (**F**) High magnification image of one of the donor-derived DRG shown in E. Scale bar: 25 μm.

cerebral hemorrhage, suggesting that vascular integrity is disrupted, concordant with the reported phenotypes in mouse. Zebrafish *reck* mutants might represent a model for studying the role of this inhibitor in vascular development, and additional phenotypes will be described elsewhere. Recently, other investigators uncovered a developmental interplay between motor neurons and the formation of the parachordal chain (Lim et al., 2011); further study of the relationship between RECK function, vasculogenesis and sensory neurogenesis might therefore be warranted. Nonetheless, expression and mosaic analysis suggest that *reck* acts within the neural crest population to regulate the formation of sensory neurons.

There are several possible explanations for what might happen in *sdp* mutants to the neural crest precursors normally fated to become DRG neurons. It is possible that cells fail to express *neurog1* and are re-specified. We previously found that in *neurog1* mutants sensory neuron precursors instead became glia by using the *neurog1:egfp* transgene to track their fates (McGraw et al., 2008). As *reck* acts upstream of the initiation of *neurog1* expression, we have no way of tracking these precursors in *reck* mutants. Although it is possible to sample the fates of individual zebrafish neural crest cells by single-cell injection, the cells that generate DRG neurons are only a small fraction of the trunk neural crest population. A possible change in fate would therefore be difficult to observe with statistical reliability. Although it would be of interest to track *reck*-expressing neural crest cells in vivo using reporter constructs, we have been unable to identify genomic elements that direct *reck* expression owing to the poor characterization of sequence surrounding its position at the end of chromosome 24.

An alternative possibility is that proliferation of DRG precursors is reduced following loss of *reck* function. Mouse embryonic fibroblasts have reduced proliferation following *Reck* depletion (Kitajima et al., 2010). However, we observed no significant difference in proliferation in *reck*-depleted neural crest cells. A third mechanism that might contribute to the *sdp* phenotype involves the death of DRG progenitors. In our time-lapse experiments, we observed a small increase in neural crest cell apoptosis during the interval of DRG neuron differentiation. However, apoptosis was undetectable in neural crest cells in either wild-type or mutant animals using histological techniques despite an abundance of nearby apoptotic cells, confirming that neural crest cell death is extremely rare (supplementary material Fig. S7, Table S2). Regardless, we do not view apoptosis of progenitors and inappropriate progenitor migration as being mutually exclusive mechanisms for DRG defects.

Table 2. Mock-injected cells can form DRG in *reck* morphant embryos, but *reck* morphant cells cannot form DRG in mock-injected embryos

			Donor contribution		
Donor	Host	*n*	Neural crest	Dorsal root ganglia	Hit rate (%)
Mock	Mock	32	14	4	28.6
Morphant	Mock	119	18	0	0.0
Mock	Morphant	15	9	5	55.6

Transplant conditions are presented along with the number of instances neural crest was targeted and the number of instances DRG were targeted. The hit rate is derived by dividing the latter number by the former. A Fisher's exact test showed that DRG formation by donor cells was not equivalent across all conditions, P=0.003, Fisher's exact test. Post-hoc analysis using Fisher's exact test and adjusted α for repeated statistical tests (α_{adj}=0.0475) revealed that the mock into mock condition exhibited more DRG targeting than the morphant into mock condition, the morphant into mock condition exhibited less DRG targeting than the mock into morphant condition, but the degree of DRG targeting in the mock into mock condition was not significantly different from that observed in the mock into morphant condition (mock>mock versus MO>mock: P=0.037; MO>mock versus mock>MO: P=0.002; mock>mock versus mock>MO: P=0.383; Fisher's exact test).

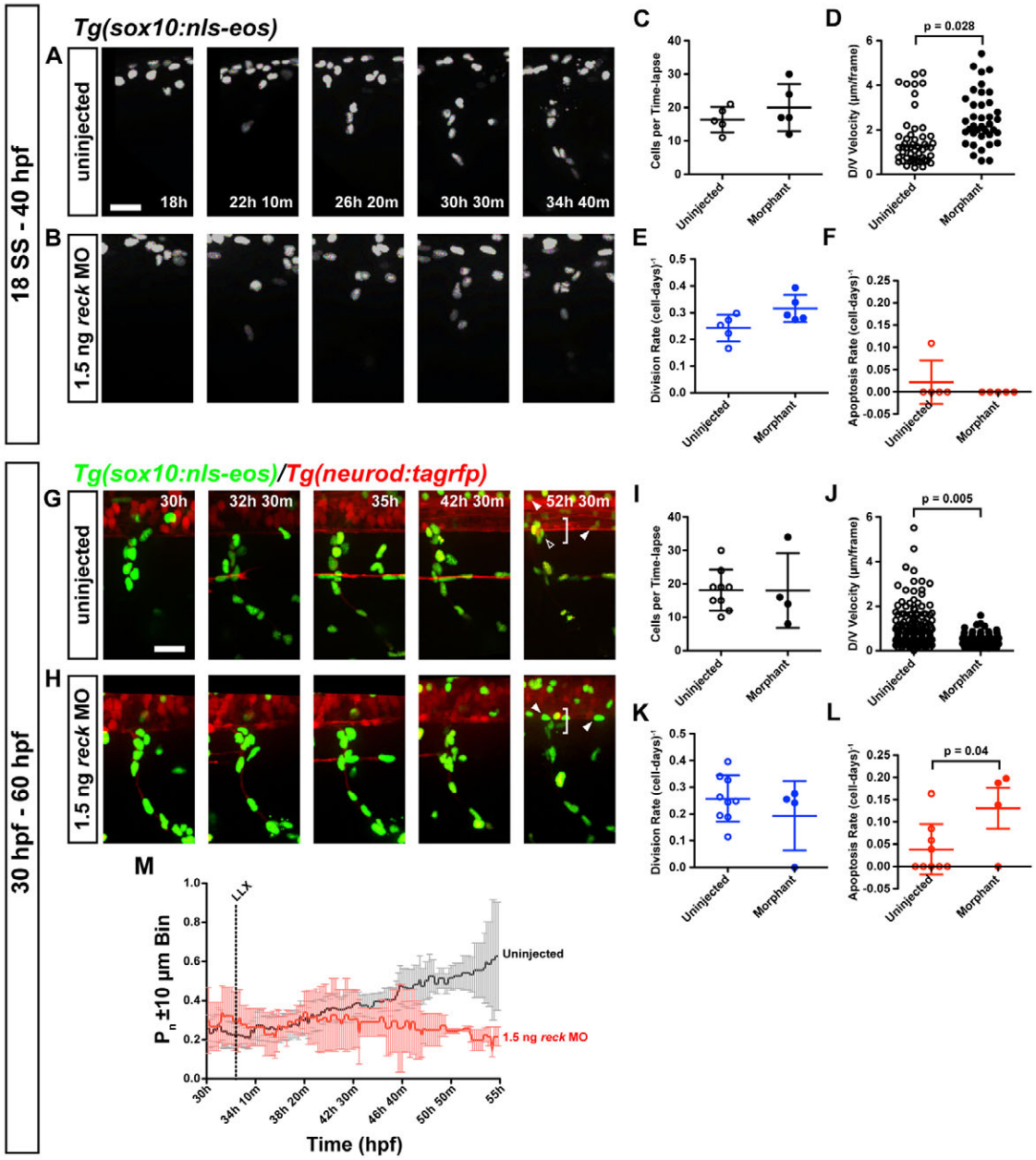

Fig. 7. Alterations in migration after *reck* depletion. (**A-F**) Uninjected and MO-injected *Tg(sox10:nls-eos)* zebrafish embryos were imaged from 18 to 40 hpf. (A,B) Migration of *reck* MO-injected neural crest is generally appropriate. Scale bar: 25 μm. (C) Number of cells is not altered after MO injection. (D) Average velocity. MO-injected cells are hypermigratory compared with uninjected cells [$t(92)=2.26$, $P=2.84E-2$]. (E) Division rate is not significantly altered following *reck* depletion. (F) Apoptosis is a rare event and was not observed in any MO-injected embryo time-lapses (preventing statistical analysis). (**G-L**) To examine cell behavior during overt DRG neuronal differentiation, uninjected and MO-injected *Tg(sox10:nls-eos)/Tg(neuroD:tagRFP)* embryos were imaged in time-lapse from 30 to 60 hpf. (G) In uninjected embryos, a subset of the cells in the migratory stream condense just ventral to the spinal cord (bin of ±10 μm is indicated by the bracket), forming the prospective DRG (empty arrowhead). These cells will become either the initial sensory neuron or its associated satellite glia. Note that *sox10*$^+$ oligodendrocytes (filled arrowheads) are visible in both conditions; they can be distinguished from neural crest by their position in the spinal cord, their spherical nuclei and their late initiation of *sox10* expression. Scale bar: 25 μm. (H) Embryos injected with 1.5 ng *reck* MO fail to form the DRG neuroglial cluster. Other neural crest cells take up positions consistent with Schwann cells or migrate out of the field entirely. (I) Number of cells tracked per time-lapse is not different in uninjected and MO-injected embryos. (J) Average velocity. MO-injected cells are hypomigratory compared with uninjected cells [$t(233)=2.79$, $P=5.6E-3$]. (K) Division rate is not significantly altered following *reck* depletion. (L) MO-injected cells undergo apoptosis at a significantly greater rate than uninjected cells [$t(11)=2.269$, $P=4.44E-2$]. (**M**) Proportion of cells inhabiting the ±10 μm bin flanking the ventralmost extent of the spinal cord at each point in time (bracket in G,H). LLX, time point at which the lateral line crosses the imaged segment. Black, uninjected embryos; red, MO-injected embryos. Error bars are ±95% confidence interval. Significantly fewer cells localize at the ventral aspect of the spinal cord. Simple linear regression of control and MO-injected data indicates that the proportion of uninjected cells inhabiting the prospective DRG microenvironment increases over time whereas the proportion of MO-injected cells inhabiting this region decreases [$F(1, 1858)=647.832$, $P<0.0001$; control: $y=2.76\times10^{-3}\,x + 0.178$; MO-injected: $y=-3.46\times10^{-4}\,x + 0.300$].

reck was first identified in a large-scale screen for cDNAs capable of returning Ras-transformed cells to a flat morphology (Takahashi et al., 1998). Subsequent work has established Reck as a regulator of cell migration and invasion (Clark et al., 2007; Noda and Takahashi, 2007). Many cancers exhibit Reck downregulation via epigenetic modifications (Chang et al., 2004; Chang et al., 2006; Chang et al., 2007), transcriptional repression (Hsu et al., 2006; Liu et al., 2003; Sasahara et al., 1999), post-translational modifications (Simizu et al., 2005) or endogenous microRNAs (Gabriely et al., 2008; Liu et al., 2010). In general, *RECK* expression is negatively correlated with tumor aggressiveness (Clark et al., 2011; Gabriely et al., 2008; Li et al., 2007; Masui et al., 2003; Rabien et al., 2007; Rabien et al., 2011; Song et al., 2006; Span et al., 2003; Takemoto et al., 2007; Takenaka et al., 2004; Takenaka et al., 2005; Takeuchi et al., 2004; van der Jagt et al., 2006; Xu et al., 2010); presumably in the absence of *RECK*, metalloproteinase hyperactivity enables greater tumor cell migration and invasion.

Like cancer cells, neural crest cells migrate through the extracellular environment to reach their final targets. One possible explanation for the DRG phenotype caused by result of *reck* loss of function is that neurogenic neural crest migrates inappropriately. We observed broad *reck* expression in neural crest cells at 22 hpf followed by restriction to a subset of neural crest cells by 30 hpf, suggesting that winnowing of *reck* expression might confer DRG progenitor identity as development progresses. We found that the requirement for *reck* is cell autonomous, a result that was somewhat surprising given the extensive expression of *reck* transcript in cells situated in the path of neural crest migration and the large increase in metalloproteinase activity in *sdp* embryos, suggesting that it is broadly active in tissues besides neural crest. Reck has been shown to inhibit metalloproteinases in cis (Muraguchi et al., 2007), suggesting that a potential metalloproteinase, the inhibition of which is crucial for normal DRG development, might be expressed within the neural crest itself, consistent with a cell-autonomous function. However, we cannot rescue the *sdp* defect by treating with several broad-spectrum inhibitors of metalloproteinases (supplementary material Fig. S9), although the efficacy of these inhibitors against specific zebrafish metalloproteinases is unknown. Whether any of the >50 zebrafish metalloproteinases interact with Reck awaits further analysis.

When viewed by time-lapse microscopy, *reck*-depleted cells exhibit changes in migratory behavior. Initially, we observed neural crest to be hypermigratory in *reck* MO-injected embryos, showing a small but significant increase in cell velocity. We note that we are unable to determine whether these differences reflect changes in behavior of all neural crest cells or only a subset. When viewed at later times, *reck*-depleted cells appear hypomigratory, in contrast to their earlier behavior. These results can be reconciled by a model in which *reck*-deficient cells initially show increased migration, as predicted from the cancer literature. In the absence of *reck* function, DRG precursors would then be re-specified (or die), leaving only slow-moving cells on the medial pathway destined to become Schwann glia. A subset of neural crest-derived *sox10*$^{+}$ cells are unambiguously mislocalized following *reck* depletion, failing to move dorsally. These include neuronal precursors and cells that will form satellite glia surrounding the DRG. However, dorsal migration occurs after initial expression of *neurog1*, and both the failure of dorsal movement to form DRG and subsequent accumulation of satellite cells might be caused indirectly by *neurog1* absence in *reck* mutants. Whether the lack of dorsal movement at this later stage is due to altered Reck function or whether it is the consequence of failed specification will await further study.

An alternative possibility for the function of *reck* in DRG specification is that altered activity of metalloproteinases could affect signaling required for neuron specification (reviewed by Bai and Pfaff, 2011). In the mouse, Reck regulates cortical neurogenesis through Notch signaling (Muraguchi et al., 2007). When Reck is disrupted, hyperactive ADAM10 results in reduced Notch signaling and precocious neurogenesis with an ultimate decrease in neurons due to precursor depletion. Might a similar impairment be the mechanism by which *sdp* embryos fail to form DRG? Disruption in Notch signaling results in a decrease in DRG (Cornell and Eisen, 2000; Cornell and Eisen, 2002), but this phenotype is the result of prior depletion in all trunk neural crest with concomitant increase in Rohon-Béard sensory neurons. We observe no change in Rohon-Béard cells in mutant embryos (supplementary material Fig. S8) and normal crest formation and differentiation (supplementary material Fig. S1). Moreover, loss of zebrafish *notch1a* receptor causes an increase in DRG neurons (Gray et al., 2001), more consistent with the neurogenic phenotype expected with loss of Notch function. Does *sdp* instead behave as a mutation resulting in Notch gain of function? We are unable to rescue DRG formation by treating *sdp* embryos with the Notch inhibitor DAPT (Geling et al., 2002) although we see an increase in DRG neurons when treating wild-type animals (data not shown), consistent with the *notch1a* mutant phenotype. Alternatively, Reck might alter other metalloproteinases that affect signaling pathways needed for DRG differentiation.

A limited body of evidence provides clues as to how *reck* might fit into a genetic hierarchy controlling DRG development. *erbb2* and *erbb3b* function have previously been shown to be essential to the formation of DRG neurons upstream of *neurog1* expression; migrating neural crest in these mutants becomes progressively disorganized and DRG precursors apparently fail to pause and differentiate (Honjo et al., 2008). ErbB2 is known to regulate Reck expression via ERK signaling (Hsu et al., 2006), and the loss of DRG observed in both *erbb2* and *reck* mutants suggests that the two genes might act within a common signaling cascade to direct DRG formation. However, mutations affecting Erbb signaling also disrupt glial development (Lyons et al., 2005), suggesting that this pathway might affect DRG development at an earlier step involving the neuroglial precursor.

Taken together, our results suggest that Reck cell autonomously regulates the initial specification of DRG precursors upstream of *neurog1*. *reck* expression is restricted to a subset of neural crest, suggesting that these cells might represent DRG precursors. DRG cell fate choice might, therefore, rely on regulation of *reck* expression. Understanding which metalloproteinases are inhibited by Reck during zebrafish neural crest development will be crucial for resolving the mechanisms underlying how it regulates neural crest cell fate.

Acknowledgements

The authors wish to thank Adrienne Mueller, William Wood and Andrew Millspaugh for their assistance in writing MatLab modules. We also wish to thank Sarah Kucenas for generously providing the anti-Sox10 antibody. We thank the Sanger Centre for help with assembly of the distal end of chromosome 24.

Funding

This investigation was supported in part by the National Institute of General Medical Sciences [NRSA 2T32 GM007270]; the National Institute of Neurological Disorders and Stroke [NS057220]; and the intramural program of

the Eunice Kennedy Shriver National Institute of Child Health and Human Development [HD001011 to B.W.]. Deposited in PMC for release after 12 months.

Competing interests statement
The authors declare no competing financial interests.

Supplementary material
Supplementary material available online at
http://dev.biologists.org/lookup/suppl/doi:10.1242/dev.072439/-/DC1

References

Andermann, P., Ungos, J. and Raible, D. W. (2002). Neurogenin1 defines zebrafish cranial sensory ganglia precursors. *Dev. Biol.* **251**, 45-58.
Bahary, N., Davidson, A., Ransom, D., Shepard, J., Stern, H., Trede, N., Zhou, Y., Barut, B. and Zon, L. I. (2004). The Zon laboratory guide to positional cloning in zebrafish. *Methods Cell Biol.* **77**, 305-329.
Bai, G. and Pfaff, S. L. (2011). Protease regulation: the yin and yang of neural development and disease. *Neuron* **72**, 9-21.
Carney, T. J., Dutton, K. A., Greenhill, E., Delfino-Machín, M., Dufourcq, P., Blader, P. and Kelsh, R. N. (2006). A direct role for Sox10 in specification of neural crest-derived sensory neurons. *Development* **133**, 4619-4630.
Chang, H.-C., Liu, L.-T. and Hung, W.-C. (2004). Involvement of histone deacetylation in ras-induced down-regulation of the metastasis suppressor RECK. *Cell Signal.* **16**, 675-679.
Chang, H.-C., Cho, C.-Y. and Hung, W.-C. (2006). Silencing of the metastasis suppressor RECK by RAS oncogene is mediated by DNA methyltransferase 3b-induced promoter methylation. *Cancer Res.* **66**, 8413-8420.
Chang, H.-C., Cho, C.-Y. and Hung, W.-C. (2007). Downregulation of RECK by promoter methylation correlates with lymph node metastasis in non-small cell lung cancer. *Cancer Sci.* **98**, 169-173.
Clark, J. C. M., Thomas, D. M., Choong, P. F. M. and Dass, C. R. (2007). RECK – a newly discovered inhibitor of metastasis with prognostic significance in multiple forms of cancer. *Cancer Metastasis Rev.* **26**, 675-683.
Clark, J. C. M., Akiyama, T., Thomas, D. M., Labrinidis, A., Evdokiou, A., Galloway, S. J., Kim, H.-S., Dass, C. R. and Choong, P. F. M. (2011). RECK in osteosarcoma. *Cancer* **117**, 3517-3528.
Cornell, R. A. and Eisen, J. S. (2000). Delta signaling mediates segregation of neural crest and spinal sensory neurons from zebrafish lateral neural plate. *Development* **127**, 2873-2882.
Cornell, R. A. and Eisen, J. S. (2002). Delta/Notch signaling promotes formation of zebrafish neural crest by repressing Neurogenin 1 function. *Development* **129**, 2639-2648.
Fisher, S., Grice, E. A., Vinton, R. M., Bessling, S. L., Urasaki, A., Kawakami, K. and McCallion, A. S. (2006). Evaluating the biological relevance of putative enhancers using Tol2 transposon-mediated transgenesis in zebrafish. *Nat. Protoc.* **1**, 1297-1305.
Gabriely, G., Wurdinger, T., Kesari, S., Esau, C. C., Burchard, J., Linsley, P. S. and Krichevsky, A. M. (2008). MicroRNA 21 promotes glioma invasion by targeting matrix metalloproteinase regulators. *Mol. Cell. Biol.* **28**, 5369-5380.
Gans, C. and Northcutt, R. G. (1983). Neural crest and the origin of vertebrates: a new head. *Science* **220**, 268-273.
Geling, A., Steiner, H., Willem, M., Bally-Cuif, L. and Haass, C. (2002). A gamma-secretase inhibitor blocks Notch signaling in vivo and causes a severe neurogenic phenotype in zebrafish. *EMBO Rep.* **3**, 688-694.
Gray, M., Moens, C. B., Amacher, S. L., Eisen, J. S. and Beattie, C. E. (2001). Zebrafish deadly seven functions in neurogenesis. *Dev. Biol.* **237**, 306-323.
Greenwood, A. L., Turner, E. E. and Anderson, D. J. (1999). Identification of dividing, determined sensory neuron precursors in the mammalian neural crest. *Development* **126**, 3545-3559.
Henion, P. D., Raible, D. W., Beattie, C. E., Stoesser, K. L., Weston, J. A. and Eisen, J. S. (1996). Screen for mutations affecting development of zebrafish neural crest. *Dev. Genet.* **18**, 11-17.
Honjo, Y., Kniss, J. and Eisen, J. S. (2008). Neuregulin-mediated ErbB3 signaling is required for formation of zebrafish dorsal root ganglion neurons. *Development* **135**, 2615-2625.
Hsu, M.-C., Chang, H.-C. and Hung, W.-C. (2006). HER-2/neu represses the metastasis suppressor RECK via ERK and Sp transcription factors to promote cell invasion. *J. Biol. Chem.* **281**, 4718-4725.
Kamei, M., Isogai, S., Pan, W. and Weinstein, B. M. (2010). Imaging blood vessels in the zebrafish. *Methods Cell Biol.* **100**, 27-54.
Kang, H.-G., Kim, H.-S., Kim, K.-J., Oh, J. H., Lee, M.-R., Seol, S. M. and Han, I. (2007). RECK expression in osteosarcoma: correlation with matrix metalloproteinases activation and tumor invasiveness. *J. Orthop. Res.* **25**, 696-702.
Kimmel, C. B., Ballard, W. W., Kimmel, S. R., Ullmann, B. and Schilling, T. F. (1995). Stages of embryonic development of the zebrafish. *Dev. Dyn.* **203**, 253-310.
Kitajima, S., Miki, T., Takegami, Y., Kido, Y., Noda, M., Hara, E., Shamma, A. and Takahashi, C. (2010). Reversion-inducing cysteine-rich protein with Kazal motifs interferes with epidermal growth factor receptor signaling. *Oncogene* **30**, 737-750.
Knecht, A. K. and Bronner-Fraser, M. (2002). Induction of the neural crest: a multigene process. *Nat. Rev. Genet.* **3**, 453-461.
Korzh, V., Sleptsova, I., Liao, J., He, J. and Gong, Z. (1998). Expression of zebrafish bHLH genes ngn1 and nrd defines distinct stages of neural differentiation. *Dev. Dyn.* **213**, 92-104.
Kwan, K. M., Fujimoto, E., Grabher, C., Mangum, B. D., Hardy, M. E., Campbell, D. S., Parant, J. M., Yost, H. J., Kanki, J. P. and Chien, C.-B. (2007). The Tol2kit: a multisite gateway-based construction kit for Tol2 transposon transgenesis constructs. *Dev. Dyn.* **236**, 3088-3099.
Lawson, N. D. and Weinstein, B. M. (2002). In vivo imaging of embryonic vascular development using transgenic zebrafish. *Dev. Biol.* **248**, 307-318.
Le Douarin. N. and Kalcheim, C. (1999). *The Neural Crest*. Cambridge, UK: Cambridge University Press.
Li, S.-L., Gao, D.-L., Zhao, Z.-H., Liu, Z.-W., Zhao, Q.-M., Yu, J.-X., Chen, K.-S. and Zhang, Y.-H. (2007). Correlation of matrix metalloproteinase suppressor genes RECK, VEGF, and CD105 with angiogenesis and biological behavior in esophageal squamous cell carcinoma. *World J. Gastroenterol.* **13**, 6076-6081.
Lim, A. H., Suli, A., Yaniv, K., Weinstein, B., Li, D. Y. and Chien, C. B. (2011). Motoneurons are essential for vascular pathfinding. *Development* **138**, 3847-3857.
Lister, J. A., Robertson, C. P., Lepage, T., Johnson, S. L. and Raible, D. W. (1999). *nacre* encodes a zebrafish microphthalmia-related protein that regulates neural-crest-derived pigment cell fate. *Development*, **126**, 3757-3767.
Liu, C., Yu, J., Yu, S., Lavker, R. M., Cai, L., Liu, W., Yang, K., He, X. and Chen, S. (2010). MicroRNA-21 acts as an oncomir through multiple targets in human hepatocellular carcinoma. *J. Hepatol.* **53**, 98-107.
Liu, L.-T., Peng, J.-P., Chang, H.-C. and Hung, W.-C. (2003). RECK is a target of Epstein-Barr virus latent membrane protein 1. *Oncogene* **22**, 8263-8270.
Lyons, D. A., Pogoda, H.-M., Voas, M. G., Woods, I. G., Diamond, B., Nix, R., Arana, N., Jacobs, J. and Talbot, W. S. (2005). erbb3 and erbb2 are essential for schwann cell migration and myelination in zebrafish. *Curr. Biol.* **15**, 513-524.
Ma, Q., Fode, C., Guillemot, F. and Anderson, D. J. (1999). Neurogenin1 and neurogenin2 control two distinct waves of neurogenesis in developing dorsal root ganglia. *Genes Dev.* **13**, 1717-1728.
Marusich, M. F., Furneaux, H. M., Henion, P. D. and Weston, J. A. (1994). Hu neuronal proteins are expressed in proliferating neurogenic cells. *J. Neurobiol.* **25**, 143-155.
Masui, T., Doi, R., Koshiba, T., Fujimoto, K., Tsuji, S., Nakajima, S., Koizumi, M., Toyoda, E., Tulachan, S., Ito, D. et al. (2003). RECK expression in pancreatic cancer: its correlation with lower invasiveness and better prognosis. *Clin. Cancer Res.* **9**, 1779-1784.
McGraw, H. F., Nechiporuk, A. and Raible, D. W. (2008). Zebrafish dorsal root ganglia neural precursor cells adopt a glial fate in the absence of neurogenin1. *J. Neurosci.* **28**, 12558-12569.
Morioka, Y., Monypenny, J., Matsuzaki, T., Shi, S., Alexander, D. B., Kitayama, H. and Noda, M. (2009). The membrane-anchored metalloproteinase regulator RECK stabilizes focal adhesions and anterior-posterior polarity in fibroblasts. *Oncogene* **28**, 1454-1464.
Muraguchi, T., Takegami, Y., Ohtsuka, T., Kitajima, S., Chandana, E. P. S., Omura, A., Miki, T., Takahashi, R., Matsumoto, N., Ludwig, A. et al. (2007). RECK modulates Notch signaling during cortical neurogenesis by regulating ADAM10 activity. *Nat. Neurosci.* **10**, 838-845.
Noda, M. and Takahashi, C. (2007). Recklessness as a hallmark of aggressive cancer. *Cancer Sci.* **98**, 1659-1665.
Oh, J., Takahashi, R., Kondo, S., Mizoguchi, A., Adachi, E., Sasahara, R. M., Nishimura, S., Imamura, Y., Kitayama, H., Alexander, D. B. et al. (2001). The membrane-anchored MMP inhibitor RECK is a key regulator of extracellular matrix integrity and angiogenesis. *Cell* **107**, 789-800.
Perez, S. E., Rebelo, S. and Anderson, D. J. (1999). Early specification of sensory neuron fate revealed by expression and function of neurogenins in the chick embryo. *Development* **126**, 1715-1728.
Rabien, A., Burkhardt, M., Jung, M., Fritzsche, F., Ringsdorf, M., Schicktanz, H., Loening, S. A., Kristiansen, G. and Jung, K. (2007). Decreased RECK expression indicating proteolytic imbalance in prostate cancer is associated with higher tumor aggressiveness and risk of prostate-specific antigen relapse after radical prostatectomy. *Eur. Urol.* **51**, 1259-1266.
Rabien, A., Ergün, B., Erbersdobler, A., Jung, K. and Stephan, C. (2011). RECK overexpression decreases invasive potential in prostate cancer cells. *Prostate* doi: 10.1002/pros.21498.
Raible, D. W. and Eisen, J. S. (1994). Restriction of neural crest cell fate in the trunk of the embryonic zebrafish. *Development* **120**, 495-503.
Rubinstein, A. L., Lee, D., Luo, R., Henion, P. D. and Halpern, M. E. (2000). Genes dependent on zebrafish cyclops function identified by AFLP differential gene expression screen. *Genesis*, **26**, 86-97.

Sasahara, R. M., Takahashi, C. and Noda, M. (1999). Involvement of the Sp1 site in ras-mediated downregulation of the RECK metastasis suppressor gene. *Biochem. Biophys. Res. Commun.* **264**, 668-675.
Silveira Corrêa, T. C., Massaro, R. R., Brohem, C. A., Taboga, S. R., Lamers, M. L., Santos, M. F. and Maria-Engler, S. S. (2010). RECK-mediated inhibition of glioma migration and invasion. *J. Cell. Biochem.* **110**, 52-61.
Simizu, S., Takagi, S., Tamura, Y. and Osada, H. (2005). RECK-mediated suppression of tumor cell invasion is regulated by glycosylation in human tumor cell lines. *Cancer Res.* **65**, 7455-7461.
Solnica-Krezel, L., Schier, A. F. and Driever, W. (1994). Efficient recovery of ENU-induced mutations from the zebrafish germline. *Genetics* **136**, 1401-1420.
Song, S. Y., Son, H. J., Nam, E., Rhee, J. C. and Park, C. (2006). Expression of reversion-inducing-cysteine-rich protein with Kazal motifs (RECK) as a prognostic indicator in gastric cancer. *Eur. J. Cancer* **42**, 101-108.
Span, P. N., Sweep, C. G. J., Manders, P., Beex, L. V. A. M., Leppert, D. and Lindberg, R. L. P. (2003). Matrix metalloproteinase inhibitor reversion-inducing cysteine-rich protein with Kazal motifs: a prognostic marker for good clinical outcome in human breast carcinoma. *Cancer* **97**, 2710-2715.
Szabo, A., Dalmau, J., Manley, G., Rosenfeld, M., Wong, E., Henson, J., Posner, J. B. and Furneaux, H. M. (1991). HuD, a paraneoplastic encephalomyelitis antigen, contains RNA-binding domains and is homologous to Elav and Sex-lethal. *Cell* **67**, 325-333.
Takahashi, C., Sheng, Z., Horan, T. P., Kitayama, H., Maki, M., Hitomi, K., Kitaura, Y., Takai, S., Sasahara, R. M., Horimoto, A. et al. (1998). Regulation of matrix metalloproteinase-9 and inhibition of tumor invasion by the membrane-anchored glycoprotein RECK. *Proc. Natl. Acad. Sci. USA* **95**, 13221-13226.
Takemoto, N., Tada, M., Hida, Y., Asano, T., Cheng, S., Kuramae, T., Hamada, J.-I., Miyamoto, M., Kondo, S. and Moriuchi, T. (2007). Low expression of reversion-inducing cysteine-rich protein with Kazal motifs (RECK) indicates a shorter survival after resection in patients with adenocarcinoma of the lung. *Lung Cancer* **58**, 376-383.
Takenaka, K., Ishikawa, S., Kawano, Y., Yanagihara, K., Miyahara, R., Otake, Y., Morioka, Y., Takahashi, C., Noda, M., Wada, H. et al. (2004). Expression of a novel matrix metalloproteinase regulator, RECK, and its clinical significance in resected non-small cell lung cancer. *Eur. J. Cancer* **40**, 1617-1623.
Takenaka, K., Ishikawa, S., Yanagihara, K., Miyahara, R., Hasegawa, S., Otake, Y., Morioka, Y., Takahashi, C., Noda, M., Ito, H. et al. (2005). Prognostic significance of reversion-inducing cysteine-rich protein with Kazal motifs expression in resected pathologic stage IIIA N2 non-small-cell lung cancer. *Ann. Surg. Oncol.* **12**, 817-824.
Takeuchi, T., Hisanaga, M., Nagao, M., Ikeda, N., Fujii, H., Koyama, F., Mukogawa, T., Matsumoto, H., Kondo, S., Takahashi, C. et al. (2004). The membrane-anchored matrix metalloproteinase (MMP) regulator RECK in combination with MMP-9 serves as an informative prognostic indicator for colorectal cancer. *Clin. Cancer Res.* **10**, 5572-5579.
Thisse, C. and Thisse, B. (2008). High-resolution in situ hybridization to whole-mount zebrafish embryos. *Nat. Protoc.* **3**, 59-69.
Ungos, J. M., Karlstrom, R. O. and Raible, D. W. (2003). Hedgehog signaling is directly required for the development of zebrafish dorsal root ganglia neurons. *Development* **130**, 5351-5362.
van der Jagt, M. F. P., Sweep, F. C. G. J., Waas, E. T., Hendriks, T., Ruers, T. J. M., Merry, A. H. H., Wobbes, T. and Span, P. N. (2006). Correlation of reversion-inducing cysteine-rich protein with kazal motifs (RECK) and extracellular matrix metalloproteinase inducer (EMMPRIN), with MMP-2, MMP-9, and survival in colorectal cancer. *Cancer Lett.* **237**, 289-297.
Vize, P. D., McCoy, K. E. and Zhou, X. (2009). Multichannel wholemount fluorescent and fluorescent/chromogenic in situ hybridization in Xenopus embryos. *Nat. Protoc.* **4**, 975-983.
Weinstein, B. M., Stemple, D. L., Driever, W. and Fishman, M. C. (1995). Gridlock, a localized heritable vascular patterning defect in the zebrafish. *Nat. Med.* **1**, 1143-1147.
Westerfield, M. (2007). *The Zebrafish Book*. Eugene, OR: University of Oregon Press.
Wiedenmann, J., Ivanchenko, S., Oswald, F., Schmitt, F., Röcker, C., Salih, A., Spindler, K.-D. and Nienhaus, G. U. (2004). EosFP, a fluorescent marker protein with UV-inducible green-to-red fluorescence conversion. *Proc. Natl. Acad. Sci. USA* **101**, 15905-15910.
Xu, J., Wu, S. and Shi, X. (2010). Expression of matrix metalloproteinase regulator, RECK, and its clinical significance in osteosarcoma. *J. Orthop. Res.* **28**, 1621-1625.
Yoshida, D., Nomura, R. and Teramoto, A. (2008). Regulation of cell invasion and signalling pathways in the pituitary adenoma cell line, HP-75, by reversion-inducing cysteine-rich protein with kazal motifs (RECK). *J. Neurooncol.* **89**, 141-150.